ELSEVIER

Journal of Crystal Growth 219 (2000) 269–276

JOURNAL OF CRYSTAL GROWTH

www.elsevier.nl/locate/jcrysgro

Hydrothermal synthesis and structural characterization of $BaTiO_3$ nanocrystals

Song Wei Lu[a], Burtrand I. Lee[a,*], Zhong Lin Wang[b], William D. Samuels[c]

[a]*Department of Ceramic and Materials Engineering, Olin Hall, P.O. Box 340907, Clemson University, Clemson, SC 29634, USA*
[b]*School of Materials Science and Engineering, Georgia Institute of Technology, Atlanta, GA 30332, USA*
[c]*Pacific Northwest National Laboratory, Richland, WA 99352, USA*

Received 28 September 1999; accepted 6 July 2000
Communicated by R.W. Rousseau

Abstract

Barium titanate ($BaTiO_3$: BT) nanocrystals were tailored by hydrothermal method in the presence of polyoxyethylene (20) sorbitan monooleate (Tween® 80) as a polymeric surface modifier at 230°C for 0.5–2 h. The mean particle size was 77.8 ± 23.5 nm by transmission electron microscopy (TEM), and 83 ± 19 nm by laser-scattering particle size analyzer. The narrow particle size distribution of the nanocrystals suggested that further growth and agglomeration of crystals have been hindered by the surface modifier. These nanocrystals were identified as metastable cubic phase BT by X-ray diffractometry (XRD) and differential scanning calorimetry (DSC). However, Raman-active modes of tetragonal phase BT were detected from Raman spectra of as-prepared nanocrystals. Large strains have been observed in TEM dark field image, indicative of a structural deformation from metastable cubic phase to tetragonal phase. The results suggest that the hydrothermally synthesized BT nanocrystals are metastable cubic phase with some tetragonality.

PACS: 61.82.Rx; 64.60.My; 77.84. − s; 81.10.Dn

Keywords: Hydrothermal method; Barium titanate; Nanocrystals; Cubic-to-tetragonal transition; Strains; Raman spectroscopy

1. Introduction

The recent development of thinner multilayer ceramic capacitors (MLCCs) has tremendously increased the demand for smaller size dielectric ceramic particles. Barium titanate ($BaTiO_3$: BT) nanocrystals have great advantages over micrometer size ceramic powders when the thickness of a single ceramic layer decreases to less than 2 μm. Low-temperature synthesis has provided an exciting possibility for high purity, homogeneous, and ultra-fine $BaTiO_3$ nanoparticles [1]. BT nanocrystals have been synthesized by using a hydrothermal method [2–18], sol–gel processing [19–24], the oxalate route [25], microwave heating [26], a micro-emulsion process [27,28], and a polymeric precursor method [29]. Reaction mechanisms and thermodynamic modeling for BT nanocrystal formation during wet-chemical processing have

* Corresponding author. Tel.: + 1-864-656-5348; fax: + 1-864-656-1453.
E-mail address: burtrand.lee@ces.clemson.edu (B.I. Lee).

0022-0248/00/$ - see front matter
PII: S0022-0248(00)00619-9

been studied [30]. Eckert et al. [5] proposed a dissolution–precipitation mechanism for hydrothermal synthesis of $BaTiO_3$ nanocrystals using $Ba(OH)_2$ and TiO_2 as precursors.

In the past years, extensive discussion has focused on crystalline phase of nanocrystalline BT particles. Three questions are raised in the literature. First, what is the critical size below which the abnormal cubic phase is stable at room temperature? The critical crystalline size has been reported as 49 nm by Schlag and Eicke [20] using X-ray diffractometry (XRD) and differential scanning calorimetry (DSC), 120 nm by Uchino et al. [31], 30 nm by Hsiang and Yen [25,32] using XRD, and 190 nm by Begg et al. [17]. The discrepancy of the critical size determination results from different synthesis methods, conditions, and experimental techniques. Second, whether the nanocrystal has a true cubic phase without any tetragonality when it appears to be cubic according XRD and DSC results? Various researchers [3,4,16–18,25,26, 32–34] assigned the BT nanocrystallites to cubic phase according to their XRD and DSC results. Cho [29] and Clark et al. [13] argued that the nanocrystalline BT particles are tetragonal rather than cubic according to the presence of Raman-active modes for the tetragonal phase. However, Beck et al. [27] observed no Raman-active mode in BT nanoparticles less than 20 nm synthesized by a micro-emulsion method. Third, whether the tetragonal phase BT nanocrystals have better sintering behaviors and higher dielectric constants than cubic phase? Zhu et al. [34] claimed that hydrothermally synthesized tetragonal BT nanocrystals have better sintering behavior, higher density, and higher dielectric constants than cubic phase nanoparticles. However, Takeuchi et al. [35,36] reported similar dense ceramics (more than 95% of theoretical density) and similar high dielectric constants from hydrothermal BT nanocrystals, for both cubic and tetragonal phases, after spark plasma sintering.

There is also a misunderstanding between particle size and crystalline size. Only when the individual particle is a single crystal, the crystalline size is same as the particle size. Yet, the debate of the phase, i.e., to cubic phase by XRD and DSC, and tetragonal phase by Raman spectroscopy, has not been concluded in the literature. It is one of the main aims for this paper to clarify the structure of BT nanocrystals synthesized by a hydrothermal method, and to confirm the BT phase.

Another issue concerning nanoparticles is the dispersion processing. Due to the large surface area to volume ratio, the tendency to agglomerate is very high. In an industrial practice, a well-dispersed BT suspension is needed to obtain a high green density of the final BT product. The second aim of this research is, therefore, to synthesize redispersible or agglomerate-free BT nanocrystals by a polymeric surface agent which controls the particle size and provides the dispersibility in water. The surface adsorbate layer formed on nanocrystal surface acts simultaneously as a surface modifier to hinder the further growth of nanoparticles [37–40], and as a dispersant to prevent the particle agglomeration by a steric stabilization in the subsequent suspension preparation.

2. Experimental procedure

An aqueous solution of barium and titanium was obtained by mixing 14.66 g $BaCl_2 \cdot 2H_2O$ (99.6%, Fischer Scientific Company) in 40 ml deionized water and 3.79 g $TiCl_4$ (99.9%, Acros Organics) in 40 ml chilled deionized water. One-half-gram of polyoxyethylene (20) sorbitan monooleate (Tween® 80) was added as the surface modifier to the above solution. The solution pH was raised to 13.5 by dropwise adding 4 M KOH with stirring, resulting in a white colloidal sol. The final volume was adjusted to 100 ml using deionized water. Thereafter, 25 ml of the sol was transferred to a 30 ml stainless-steel vessel. The sealed vessel was heated to 230°C for 0.5–2 h. After cooling down to room temperature, the resultant precipitate was centrifuged and washed with water for several times, and finally dried at 60°C for 24 h in a vacuum oven. Excess Ba^{2+} and KOH were removed during washing. A high purity 99.995% BT powder from Aldrich chemical Company was used as a reference.

Transmission electron microscopy (TEM) study of the synthesized BT nanocrystals was carried out at 200 kV using a Hitachi HF-2000 TEM equipped with a field emission source and at 400 kV using

a JEOL 4000EX. Energy dispersive X-ray spectroscopy (EDS) attached onto the Hitachi HF-2000 TEM was used to determine the chemical composition of the sample. The TEM specimens were prepared by dispersing the as-prepared BT particles in methane, and picking up using a carbon film supported by a copper grid. The particle size and size distribution were characterized using a Horiba LA-910 laser-scattering particle size analyzer. The samples were dispersed in distilled water and ultrasonically treated for 10 min before the size analysis. XRD measurements were performed using an XDS X-ray diffractometer (Model 2000, Scintag, Inc.) from $2\theta = 20$–80° with a scan step of 0.02°. Raman investigations were carried out by means of an SPEX 1877 Triple Raman Spectrometer equipped with a Princeton Instruments LN/CCD detector and an SPEX 1482ET Micramate microscopy attachment. The samples were excited using a coherent Innova 307 Ar^+ laser at 514.5 nm at 10 mW. DSC experiment was performed by using a Perkin-Elmer differential thermal analyzer DTA7 in air from 80 to 155°C with a heating rate of $10^\circ C\,min^{-1}$. Thirty milligram BT nanocrystals were weighed out into an alumina crucible against the same amount of pure Al_2O_3 powder as a reference.

3. Results and discussion

Fig. 1 shows XRD patterns of BT nanocrystals hydrothermally synthesized at 230°C for 0.5 and 2 h. The insert represents the enlarged pattern between $2\theta = 44.0$ and 46.0° of 2 h sample. The vertical lines indicate the peak positions of standard cubic phase BT JCPDS No. 31-174.

It is shown in Fig. 1 that both patterns fit well with the peak positions of standard cubic-phase BT. From the inset, the single peak at $2\theta = 44.95^\circ$ fits very well with the $\{2\,0\,0\}$ plane of cubic-phase BT. No split of the $\{2\,0\,0\}$ peak around $2\theta = 44.95^\circ$ can be seen in the insert. It can be unmistakably distinguished from tetragonal BT phase, since there are two overlapping peaks at 44.85 and 45.38° for tetragonal BT [3,4,33]. In order to give a clear view of this $\{2\,0\,0\}$ peak, a Gaussian fitting is performed in Fig. 2, i.e., for the peak C. The Gaussian-fitting

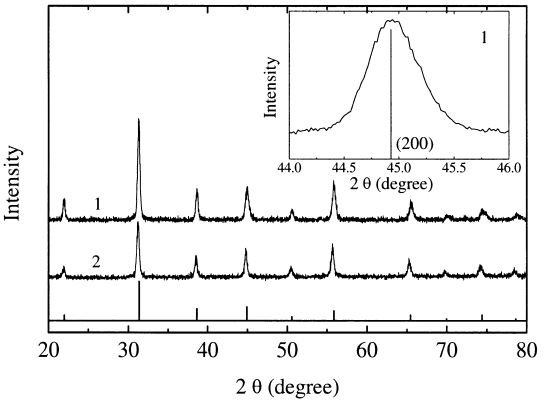

Fig. 1. XRD patterns of BT nanocrystals prepared at 230°C for (1) 2 h and (2) 0.5 h. The inset represents the enlarged XRD patterns between 44.0 and 46.0° of pattern 1. The vertical lines were taken from standard cubic phase BT JCPDS No. 31-174.

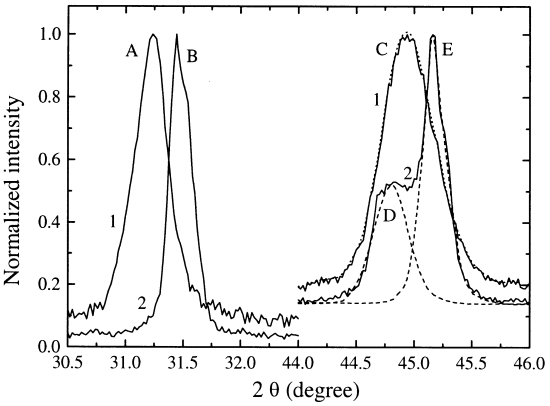

Fig. 2. Peak broadening of BT nanocrystals and peak split of the tetragonal phase: (1) BT nanocrystals, (2) tetragonal phase reference BT (micrometer size). Full-width at half-maximum (FWHM) of all peaks (A) 0.34°, (B) 0.22°, (C) 0.47°, (D) 0.31°, and (E) 0.22°.

curve of peak C (dotted line) fits very well with the original XRD pattern.

By comparison with XRD pattern of micrometer reference BT powders in Fig. 2, both peak split of micrometer size BT and peak broadening of BT nanocrystals are noticed. As previously mentioned, the split of the peak to D and E in Fig. 2 from micrometer is a characteristic indication of the tetragonal phase BT [3,4,33]. Two overlapped Gaussian peaks are the $\{0\,0\,2\}$ and $\{2\,2\,0\}$ peaks of

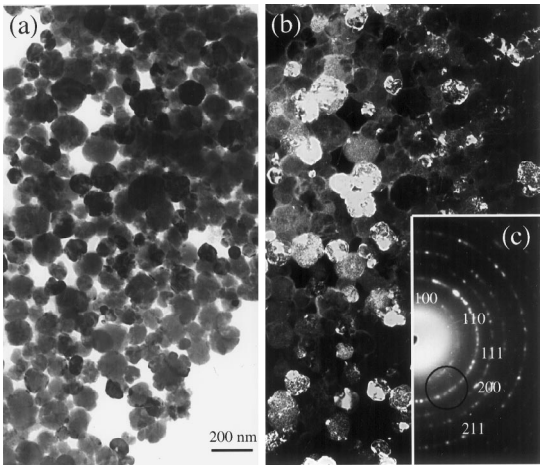

Fig. 3. (a) Bright-field and (b) dark-field TEM images recorded from $BaTiO_3$ nanocrystals. (c) An electron diffraction pattern from the particles showing the perovskite structure. The circle indicates the size and position of the objective aperture used to record the dark-field image displayed in (b).

tetragonal phase BT. From Fig. 2, the full-width at half-maximum (FWHM) are 0.34° for peak A, 0.22° for peak B, 0.47° for peak C, 0.31° for peak D, and 0.22° for peak E. It is shown that the FWHM of nanocrystalline BT is larger than that of micrometer BT, indicative of the presence of small crystals. According to above XRD results, the hydrothermally synthesized BT nanocrystals are believed to be metastable cubic phase.

Fig. 3 shows TEM images of BT nanoparticles synthesized at 230°C for 0.5 h. The bright field image in Fig. 3(a) shows a narrow-distribution spherical nanoparticles. This bright-field TEM image was recorded using a small objective aperture that selects only the (0 0 0) central transmitted beam. The particles are found to be single crystalline, additionally proven by high-resolution lattice imaging of individual particles. The dark-field image was recorded using a smaller objective aperture that selects the part of the $\{1\,0\,0\}$ and $\{1\,1\,0\}$ reflections, as indicated by a circle in Fig. 3(c). The corresponding dark-field image given in Fig. 3(b) clearly shows high strains in each particle. The large strain in the TEM photograph is indicated by the contrast variation across a particle. If the particle is single crystalline and has no strain, it should be uniform in contrast. However, for a single-crystalline particle, if the image shows dark-bright variation in contrast, it is likely to have a high strain. Strain affects the diffraction behavior of the electrons, resulting in dramatic contrast change.

It is well known that BT as a perovskite material undergoes a cubic-to-tetragonal phase transition around the Curie point 130°C [41–43]. The tetragonal phase is the only thermodynamically stable phase of bulk BT material at room temperature. The TiO_6 structure has to be completely distorted in the tetragonal BT with a displacement of the Ti ion in its oxygen coordination octahedron for 0.12 Å and an oxygen displacement about 0.03 Å [43]. However, in BT nanocrystals, the distortion of TiO_6 structure leading to a cubic-to-tetragonal phase transition by cooling the sample through the Curie point is not possible. This is because the nanocrystals are so small that structural defects in the particles prevent the completion of the structural transition, leading to high strains within the crystals. These internal stains are due to the cubic-to-tetragonal deformation, representing a small amount of tetragonality within the nanocrystals. Since there are high strains inside the nanocrystals, the distortion of the cubic structure does occur, yet do not lead to an entire distortion to the tetragonal structure. These strains are from defects of BT nanoparticles formed during the hydrothermal synthesis, primarily in the form of lattice OH^- ions and their compensation by cation vacancies [9,13,16]. Viekanandan and Kutty [9] suggested that strains in the crystallites are related to the point defects in the lattice. Compensation of the residual hydroxyl ions in the oxygen sublattice by cation vacancies results in strains leading to the presence of metastable cubic phase at room temperature [9]. Clark et al. [13] observed that as-prepared powders contain many defects, primarily in the form of lattice OH^- ions. Shi et al. [16] also reported that the stabilization of BT cubic phase by hydrothermal method is caused by surface defects that include OH^- defects and barium vacancies.

Fig. 4 demonstrates the TEM bright field and dark field images of four individual BT nanocrystals. Four types of different contrasts resulting from different strains in BT nanocrystals are observed. BT nanocrystal (a) in the dark field of Fig. 4 has

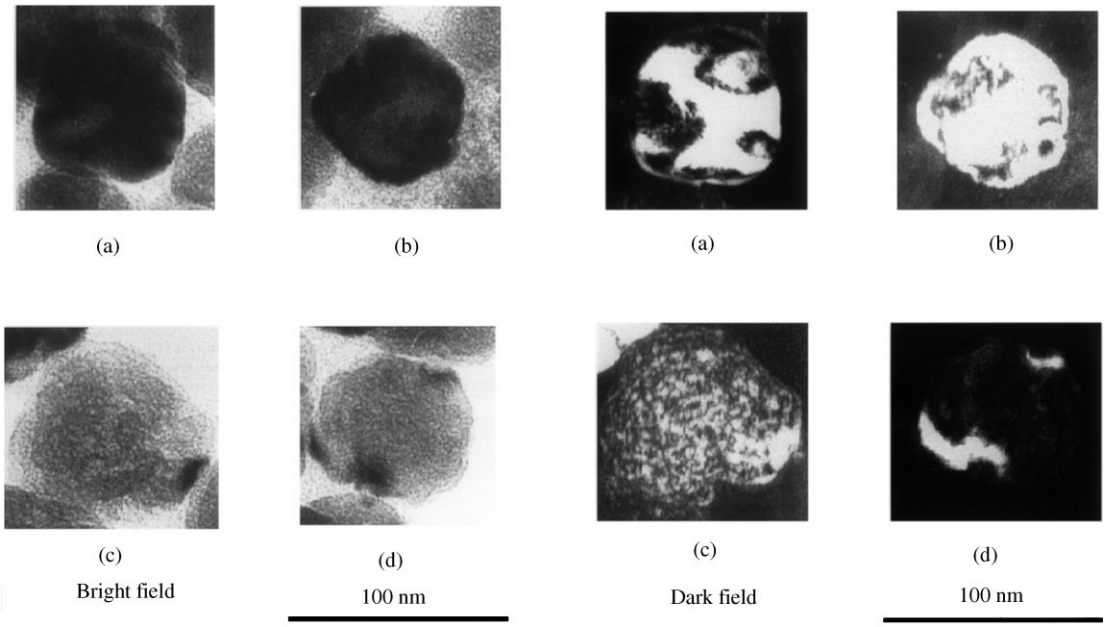

Fig. 4. TEM bright- and dark-field images of four individual BT nanocrystals with different contrasts resulting from different strains in the dark field image: (a) nearly half-bright color and half-dark color contrast; (b) bright color dominant contrast; (c) equal bright-dark color contrast with nearly homogeneous distribution; and (d) dark color dominant contrast.

a nearly half-bright and half-dark color contrast. Nanoparticle (b) has a bright color dominant contrast with some dark colors. BT particle (c) exhibits of an equal bright–dark color contrast with nearly homogeneous distribution. The fourth particle (d) has a dark color dominant contrast with some bright colors. Four different types of contrasts in Fig. 4 suggest that the high strains in four BT nanocrystals are different.

In Fig. 3(c), the electron diffraction pattern identifies that the particles are $BaTiO_3$, where the diffraction rings correspond well to the perovskite structure. EDS analysis was carried out by focusing a fine electron probe of ~ 5 nm in diameter onto a single BT particle. The EDS result exhibited Ba, Ti, and O from nanocrystals in the stoichiometric amount.

The particle size was statistically estimated to be 77.8 ± 23.5 nm from approximately 250 particles in TEM bright field image in Fig. 3(a). The particle size and size distribution measured by laser scattering method was 83 ± 19 nm. The small particle size and narrow size distribution of nanocrystals in the TEM image suggest that further growth and agglomeration of BT nanocrystals have been hindered in the presence of polymer coatings. During nucleation and crystallization of BT nanocrystals, Tween® 80 acted as a surface modifier and then a particle growth inhibitor [37–40]. The presence of these polymeric species on BT prevents the agglomeration of particles and hinders further growth of individual particles. The polymeric species remaining on BT particle surface act as a dispersant in water, leading to a well-dispersed suspension without additional dispersant as demonstrated in our previous work [44].

Since there is a cubic-to-tetragonal phase transition of BT crystals around the Curie point at 130°C, an endothermic peak in DSC curves is expected while cooling micrometer size BT powders. However, if the hydrothermally synthesized BT nanoparticles are cubic, there will be no phase transition and no endothermic peak around 130°C. Fig. 5 shows the DSC results of BT nanoparticles

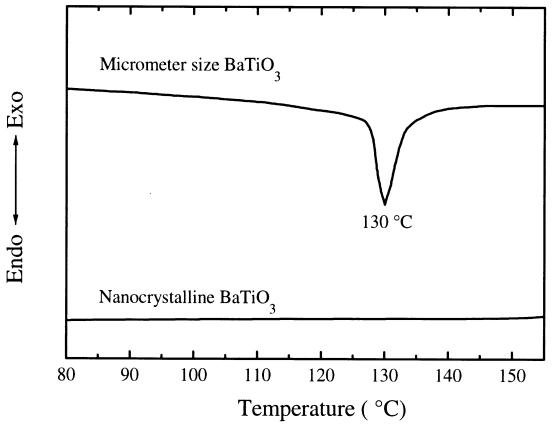

Fig. 5. DSC curves from BT nanocrystals synthesized at 230°C for 0.5 h and tetragonal BT powder.

synthesized at 230°C for 0.5 h and the tetragonal reference BT. As one can expect, there is no endothermic peak between 80 and 155°C. The absence of the enthalpy peak around the Curie point indicates no phase transition around 130°C. It is in good agreement with the attribution of cubic phase from XRD pattern at room temperature. In contrast, there is an endothermic peak in tetragonal BT.

The absence of the endothermic peak around 130°C may lead to a conclusion that the synthesized nanocrystal is cubic phase BT. However, one must be very careful to make this conclusion solely based on DSC or XRD results. Begg et al. [17] reported that the DSC endothermic peak disappeared when the $BaTiO_3$ having a tetragonality c/a less than 1.0061. This suggests that there should be no endothermic peak if the tetragonality is small. It is true that DSC technique is not very sensitive to the presence of small amount of tetragonality in the sample. Dutta et al. [33] used DSC technique to quantify the percentage of tetragonal phase in hydrothermal BT after correlating the change in enthalpy (ΔH) of the tetragonal-to-cubic transition with the amount of tetragonality in the nanocrystals. Based on the above reason, Dutta et al.'s method cannot be deemed reliable.

Hence, the determination of cubic phase BT by XRD and DSC cannot exclude the presence of a small amount of tetragonality in the nanocrystals, since both methods are not sensitive enough. Cho [29] reported that even BT particles of 20 nm size may have tetragonal asymmetry based on Raman-active modes observed for tetragonal BT in his as-prepared BT nanocrystals. Clark et al. [13] found that the presence of a peak at 305 cm^{-1} in Raman spectra indicating asymmetry within the TiO_6 octahedra of $BaTiO_3$ demonstrated clearly, on a local scale, that as-prepared BT powders do not have cubic symmetry. Therefore, they claimed that the wet-chemically synthesized BT powders are tetragonal rather than cubic. Several other researchers also reported the observation of Raman-active modes from BT nanoparticles prepared by wet-chemical techniques [10,12]. However, Busca et al. [10] explained the apparent contradiction between XRD and Raman arising from the microscopic nature of vibrational spectroscopy in contrast to the longer range order necessary to have a given X-ray diffraction pattern.

In fact, Raman spectroscopy is a highly sensitive spectroscopic technique to probe the local structure of atoms in materials. Based on crystallography, only infrared active bands without first-order Raman activity are predicated for cubic BT with a space group of Pm3 m [12,45]. However, eight Raman-active modes, seven of which are also IR active, are expected for tetragonal BT with a space group of P4 mm [12]. Hence, only active modes of tetragonal phase will be detected from Raman spectroscopy.

Fig. 6 shows the Raman spectra of as-prepared BT nanocrystals measured at 25 and 150°C, and of fired nanocrystalline BT samples (1000°C for 5 h in air) measured at 25°C. It is shown in Fig. 6 that there are several Raman-active modes resulting from the tetragonal phase for as-prepared BT nanocrystals. However, no Raman-active mode was observed at 150°C. This suggests that the BT nanocrystal is all cubic phase at 150°C [22], while at room temperature there exists some tetragonal phase. For samples after fired at 1000°C for 5 h in air, all Raman-active modes still exist similar to those of as-prepared samples. In Fig. 6, the bands around 515 and 260 cm^{-1} are assigned to the transverse optical (TO) modes of A_1 symmetry, whereas the band around 300 cm^{-1}, which is characteristic

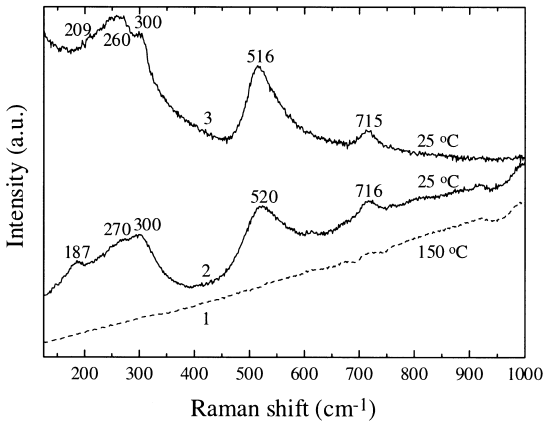

Fig. 6. Raman spectra of as prepared BT nanocrystals measured at 25 and 150°C (curves 1 and 2), and fired BT samples (1000°C for 5 h in air) measured at 25°C (curve 3).

of the tetragonal phase, is assigned to the B_1 mode. This 300 cm^{-1} peak is reduced its sharpness and becomes indistinct when the tetragonal phase is not dominant. The weak peak at 300 cm^{-1} suggests that the tetragonal phase is not the dominant phase within the synthesized nanocrystals. By the Raman-active modes, one can conclude that tetragonal phase BT exists in the hydrothermally synthesized samples. However, the tetragonal phase is not the dominant phase since the characteristic peak of tetragonal structure at 303 cm^{-1} is indistinct.

4. Conclusions

Barium titanate nanocrystals with mean size of 77.8 ± 23.5 nm were synthesized by using a hydrothermal method. XRD and DSC results indicate cubic structure of BT nanocrystals. The appearance of indistinct Raman-active modes shows the presence of non-dominant tetragonal phase. The observation of high strains from TEM dark field image agrees well with the appearance of small amount of tetragonality. The high strain is caused by lattice defects such as OH^- and their compensation by cation vacancies. The BT nanocrystals are of metastable cubic phase with some tetragonality.

Acknowledgements

This work was supported by the National Science Foundation (NSF) under the grant number DMR-9731769. We are grateful to the Raman experiments performed by Dr. C. Windisch of Pacific Northwest National Laboratory.

References

[1] P.P. Phule, S.H. Risbud, J. Mater. Sci. 25 (1990) 1169.
[2] D. Hennings, G. Rosenstein, H. Schreinemacher, J. Eur. Ceram. Soc. 8 (1991) 107.
[3] M. Wu, R. Xu, S.H. Feng, L. Li, D. Chen, Y.J. Luo, J. Mater. Sci. 31 (1996) 6201.
[4] C.T. Xia, E.W. Shi, W.E. Zhong, J.K. Guo, J. Eur. Ceram. Soc. 15 (1995) 1171.
[5] J.O. Eckert Jr., C.C. Hung-Houston, B.L. Gersten, M.M. Lencka, R.E. Riman, J. Am. Ceram. Soc. 79 (1996) 2929.
[6] E.B. Slamovich, I.A. Aksay, J. Am. Ceram. Soc. 79 (1996) 239.
[7] A.N. Christensen, Acta Chem. Scand. 24 (1970) 2447.
[8] L. Zhao, A.T. Chien, F.F. Lapse, J.S. Speck, J. Mater. Res. 11 (1996) 1325.
[9] R. Viekanandan, T.R.N. Kutty, Powder Tech. 57 (1989) 181.
[10] G. Busca, V. Buscaglia, M. Leoni, P. Nanni, Chem. Mater. 6 (1994) 955.
[11] T. Noma, S. Wada, M. Yano, T. Suzuki, J. Appl. Phys. 80 (1996) 5223.
[12] R. Asiaie, W. Zhu, S.A. Akbar, P.K. Dutta, Chem. Mater. 8 (1996) 226.
[13] I.J. Clark, T. Takeuchi, N. Ohtori, D.C. Sinclair, J. Mater. Chem. 9 (1999) 83.
[14] D. Hennings, S. Schreinemacher, J. Eur. Ceram. Soc. 9 (1992) 41.
[15] J. Menashi, R.C. Reid, L. Wagner, Cabot Corporation, US patent 4829033, May 9, 1989.
[16] E.W. Shi, C.T. Xia, W.E. Zhong, B.G. Wang, C.D. Feng, J. Am. Ceram. Soc. 80 (1997) 1567.
[17] B.D. Begg, E.R. Vance, J. Nowotny, J. Am. Ceram. Soc. 77 (1994) 3186.
[18] P.K. Dutta, J.R. Gregg, Chem. Mater. 4 (1992) 843.
[19] M.H. Frey, D.A. Payne, Phys. Rev. B 54 (1996) 3158.
[20] S. Schlag, H.F. Eicke, Solid State Commun. 91 (1994) 883.
[21] R.N. Viswanath, S. Ramasamy, Nanostruct. Mater. 8 (1997) 155.
[22] H. Shimooka, M. Kuwabara, J. Am. Ceram. Soc. 79 (1996) 2983.
[23] G. Pfaff, J. Mater. Chem. 2 (1992) 591.
[24] T. Takeuchi, M. Tabuchi, K. Ado, K. Honjo, O. Nakamura, H. Kageyama, Y. Suyama, N. Ohtori, M. Nagasawa, J. Mater. Sci. 32 (1997) 4053.
[25] H.I. Hsiang, F.S. Yen, J. Am. Ceram. Soc. 79 (1996) 1053.

[26] Y. Ma, E. Vileno, S. Suib, P.K. Dutta, Chem. Mater. 9 (1997) 3023.
[27] Ch. Beck, W. Hartl, R. Hempelmann, J. Mater. Res. 13 (1998) 3174.
[28] J. Wang, J. Fang, S.C. Ng, L.M. Gan, C.H. Chew, X. Wang, Z. Shen, J. Am. Ceram. Soc. 82 (1999) 873.
[29] W.S. Cho, J. Phys. Chem. Solid 59 (1998) 659.
[30] M.M. Lencha, R.E. Riman, Chem. Mater. 5 (1993) 61.
[31] K. Uchino, E. Sadanaga, T. Hirose, J. Am. Ceram. Soc. 72 (1989) 1555.
[32] F.S. Yen, H.I. Hsiang, Y.H. Chang, Jpn. J. Appl. Phys. Pt. 1 34 (1995) 6149.
[33] P.K. Dutta, R. Asiaie, S.A. Akbar, W. Zhu, Chem. Mater. 6 (1994) 1542.
[34] W. Zhu, S.A. Akbar, R. Asiaie, P.K. Dutta, Jpn. J. Appl. Phys. 36 (1997) 214.
[35] T. Takeuchi, M. Tabuchi, H. Kageyama, J. Am. Ceram. Soc. 82 (1999) 939.
[36] T. Takeuchi, E. Betourne, M. Tabuchi, H. Kageyama, Y. Kobayashi, A. Coats, F. Morrison, D.C. Sinclair, A.R. West, J. Mater. Sci. 34 (1999) 917.
[37] A.J.I. Ward, S.E. Friberg, J. Mater. Educ. 13 (1991) 113.
[38] P.K. Sharma, M.H. Jilavi, D. Burgard, R. Nass, H. Schmidt, J. Am. Ceram. Soc. 81 (1998) 2732.
[39] P.K. Sharma, R. Nass, H. Schmidt, Opt. Mater. 10 (1998) 161.
[40] C. Goebbert, M.A. Aegerter, D. Burgard, R. Nass, H. Schmidt, J. Mater. Chem. 9 (1999) 253.
[41] W.D. Kingery, H.K. Bowen, D.R. Uhlmann, Introduction to Ceramics, 2nd edition, Wiley, New York, 1976, p. 969.
[42] B. Jaffe, W.R. Cook Jr., H. Jaffe, Piezoelectric Ceramics, Academic Press, London and New York, 1971, p. 54.
[43] L.L. Hench, J.K. West, Principles of Electronic Ceramics, Wiley, New York, 1990, p. 246.
[44] S.W. Lu, B.I. Lee, Z.L. Wang, in: K.M. Nair, A.R. Bhalla (Eds.), Dielectric Materials & Devices, 2000, pp. 5–16. Ceramic Transaction, Vol. 106, American Ceramic Society, Westerville, OH, in press.
[45] M. Didomenico Jr., S.H. Wemple, S.P.S. Porto, R.P. Bauman, Phys. Rev. 174 (1968) 522.